Hindawi
Advances in Condensed Matter Physics
Volume 2022, Article ID 2149190, 8 pages
https://doi.org/10.1155/2022/2149190

Research Article

Thermal Spin Transport Properties in Diarylethene-Based Molecule Devices

Gang Xu,[1] **Xingyi Tan**,[1,2] **and Dahua Ren**[2]

[1]*Department of Physics, Chongqing Three Gorges University, Wanzhou 404100, China*
[2]*School of Information Engineering, Hubei Minzu University, Enshi City 445000, China*

Correspondence should be addressed to Xingyi Tan; tanxy@sanxiau.edu.cn

Received 24 June 2022; Revised 27 July 2022; Accepted 31 August 2022; Published 22 September 2022

Academic Editor: Sergio Ulloa

Copyright © 2022 Gang Xu et al. This is an open access article distributed under the Creative Commons Attribution License, which permits unrestricted use, distribution, and reproduction in any medium, provided the original work is properly cited.

Spin caloritronic devices, as multifunctional devices, combining spintronics, and caloritronics, are essential for the sustainable development of humans. Here, a novel spin caloritronic device is presented using a diarylethene molecule photoswitch sandwiched among two semi-infinite zigzag graphene nanoribbons containing asymmetrical edge hydrogenation electrodes. We demonstrate that the temperature gradient between the right and the left electrodes can generate spin-up (SU) and spin-down (SD) currents moving in opposite orientations. Moreover, the mentioned currents possess approximately the same magnitudes, indicating a nearly nondissipative spin Seebeck effect. We also find that these currents are significantly dissimilar for the two photochromic isomers at different temperature gradients, demonstrating the excellent system's switching nature. The obtained results reveal that the light can control the thermal spin transport properties.

1. Introduction

Spin caloritronics, focusing on the interconnection between heat currents and spin and taking advantage of spintronics and thermoelectronics, has stimulated much recent interest [1–8]. The mentioned field has emerged since the study of Uchida et al. [3] observed the spin Seebeck effect (SSE) in a ferromagnetic metal (NiFe alloy). This novel phenomenon substantially enhances studies on novel green energy of thermoelectricity and low-power-consumption devices. Thus, various studies have been devoted to controlling SSE using the external physical field. For instance, Ni et al. [9] found SSE in the zigzag graphene nanoribbon heterojunction by applying a sufficiently strong magnetic field. Fu et al. [10] utilized the MoS_2 monolayer or bilayer intercalated by TiP single-molecule magnets to construct spin caloritronic devices. It was found that the spin-Seebeck currents could be driven in numerous MoS_2 layers while applying a temperature gradient to the TiP-MoS_2-bilayer device and regulating the external electric field orientation. However, finding a new physical field to control the SSE is an exciting area of spin caloritronics research.

On the other hand, as photochromic molecules, photoswitches withstand a reversible transformation between their corresponding stable and metastable isomers caused by light [11]. A different light wavelength is usually employed to return to nature and generate a more thermodynamically stable isomer. Among them, diarylethene, exhibits a photochromic, thermally irreversible reactivity [12]. They often show light-influenced switching in solution and individual crystals through reversibly varying aromaticity within the open-closed (closed-open) transitions, determined by visible ultraviolet lights, respectively [13, 14]. The mentioned feature has increased the interest in studying the derivatives of diarylethene as potential photochromic molecular switches [15, 16]. Theoretically, Motta et al. [17] obtained the conductivity of two isomers of molecules based on diarylethene as well as the verification of the function of the graphene leads. They found that the switch could work electrically by applying short pulses. Photochromic diarylethene derivatives have been verified on single-walled carbon nanotube (SWCNT) as outlook single-molecule devices containing more precisely described connections to the electrodes. Experimentally, Jia et al. [18] successfully constructed

photoswitches through graphene nanoribbon (GNR) electrodes and molecules of diarylethene having a dual-mode switch performance, driven by electric field and light with significant precision and repeatability. However, to the best of our knowledge, spin caloritronic devices constructed by diarylethene-based molecules have not been reported.

The current study employed diarylethene-based molecules and zigzag graphene nanoribbons to construct spin caloritronic devices. From the theoretical computations, the spin-dependent currents could be driven by applying a temperature gradient to these devices.

2. Computational Approach

In the Atomistix ToolKit (ATK) package, spin density functional theory was combined with the nonequilibrium Green's function technique to perform electronic structures and geometrical optimization calculations [19, 20]. To determine the exchange-correlation potential, the double numerical plus polarization (DNP) basis set and the generalized gradient approximation (GGA) technique were utilized [21, 22]. To enable the convergence of the optimization, the spatial locations of the atoms were relaxed, and the maximum force tolerance was set to 0.01 eV/Å. The standard for energy convergence and the cut-off energy were selected as 1×10^{-5} eV and 150 Hartree, respectively. In order to derive the thermal spin-related transport currents, similar core electrons, cut-off energy, and exchange-correlation potentials were chosen. A $1 \times 1 \times 100$ Monkhorst-Pack k-point grid was employed to achieve precise outcomes.

In the Landauer–Büttiker formalism, the subsequent relation can be employed to derive the devices' spin-related currents [23]

$$I^{\uparrow(\downarrow)} = \frac{e}{h} \int_{-\infty}^{\infty} \left\{ T^{\uparrow(\downarrow)}(E) \left[f_L(E, T_L) - f_R(E, T_R) \right] \right\} d\mathrm{E}, \quad (1)$$

where e describes the charge of an electron, h stands for the Planck constant, $T_{L(R)}$ describes the temperature of the left (right) electrode, and $f_{L(R)}(E, T_{T(R)})$ stands for the average Fermi–Dirac distribution (FDD) of the left (right) electrode, described as follows:

$$f_{L(R)}\left(E, T_{L(R)}\right) = \left\{ 1 + \exp\left[\frac{\left(E - \mu_{L(R)}\right)}{k_B T_{L(R)}} \right] \right\}^{-1}, \quad (2)$$

where $\mu_{L(R)}$ and $T_{L(R)}$ stand for the chemical potential of the left (right) electrode and temperature, respectively, k_B denotes the Boltzmann constant, and $T^{\uparrow(\downarrow)}(E)$ indicates the spin-related transport parameter described as follows:

$$T^{\uparrow(\downarrow)}(E) = Tr\left[\Gamma_L G^r \Gamma_R G^a \right], \quad (3)$$

where $G^{r(a)}$ stands for the central area's retarded (advanced) Green's function, and $\Gamma_{L(R)}$ describes the interconnection between a central dispersion region and the left/right contact. In our system, the left electrode's temperature (T_L) is more significant than the right (T_R), while the temperature difference described as $\Delta T = T_R - T_L$ generates the thermal spin-related currents. Additionally, the previous studies found that the disorder can increase the phonon scattering and decrease the lattice thermal conductance [24, 25]. The central dispersion area (diarylethene molecule) breaks the spatial symmetry of the nanoribbons, which increases the phonon scattering and decreases the lattice thermal conductance. At the same time, it should be noted that the electron-phonon coupling is weak in ZGNRs [26], and the electron-phonon mean-free path in ZGNRs is tens of microns at room temperature [27]. Therefore, the lattice thermal conductance and the electron-phonon interaction were ignored in our calculations.

3. Results and Discussion

First, the open and closed frameworks of two different diarylethene molecules were verified, as presented in Figure 1(a). Upon ultraviolet light irradiation, the ring-open colorless diarylethene molecules undergo electrocyclization to form a ring-closed isomer that can be transformed back.

To the ring-open structure with visible light [13, 14], as shown in Figure 1(a), all molecules have similar central diphenylmethane components, connected to the electrodes via-R-with R = CO–NH (denoted by R1) and $R = CH_2$ (indicated by R2). The graphene electrodes have zigzag edges containing one edge C atom fulfilled by single H atoms and various edge C atoms fulfilled by double H atoms. One edge C atom is sp^2 hybridized and the other edge C atoms are sp^3 hybridized, as presented in Figure 1(b). Figure 1(b) presents the molecular switch's schematic diagram. The molecules of diarylethene are covalently connected to two 6-ZGNR electrodes with six zigzag carbon chains along with their width. The considered system is categorized into three components: the central dispersion area, the right electrode, and the left electrode. A supercell containing three repeated carbon modules along with the transport orientation (Z-orientation) is employed to describe the semi-infinite electrodes. The central dispersion area involves a part of the semi-infinite ZGNR electrodes, in which a screen impact happens. A supercell containing a significant vacuum layer (15 Å) in the x- and y-orientations is utilized to remove interactions from the near neighbors. Before performing electronic transport calculations, the central dispersion area is entirely relaxed through a force convergence criterion of 0.02 eV/Å.

Next, we concentrate on the zero-bias transmission spectra (TS) of open and closed isomers (R1 and R2), as presented in Figure 2. Apparently, each transmission spectra have two transmission peaks and a noticeable transmission gap can be observed near the Fermi level, while the 6-ZGNR band structures (shown in Supplementary materials Figure S1) induce the mentioned transmission properties. Figure 2 presents the spin-down (SD) electrons' transmission in a range of energies higher than the Fermi level (FL). Thus, there exists an SD negative current for this range. Besides, the behaviors of spin-up (SU) and SD currents are opposite, while there is an SU positive current. The differences between the four devices are that the closed isomers' transmission coefficients are very higher than open isomers, while the transmission channel of closed isomers is a little

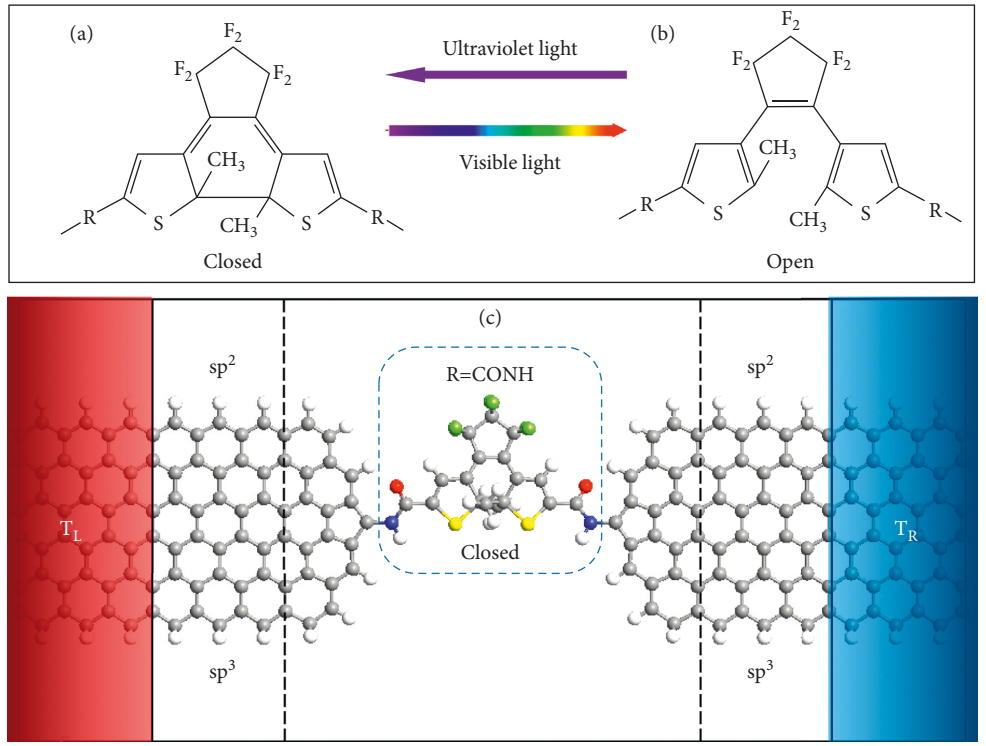

Figure 1: (a) The studied diarylethene derivative frameworks closed and open states. R stands for the functional class that connects the molecule to graphene, equal to CH_2 or CONH. (b) The thermal spin device's schematic description (R = CONH, closed state as an example).

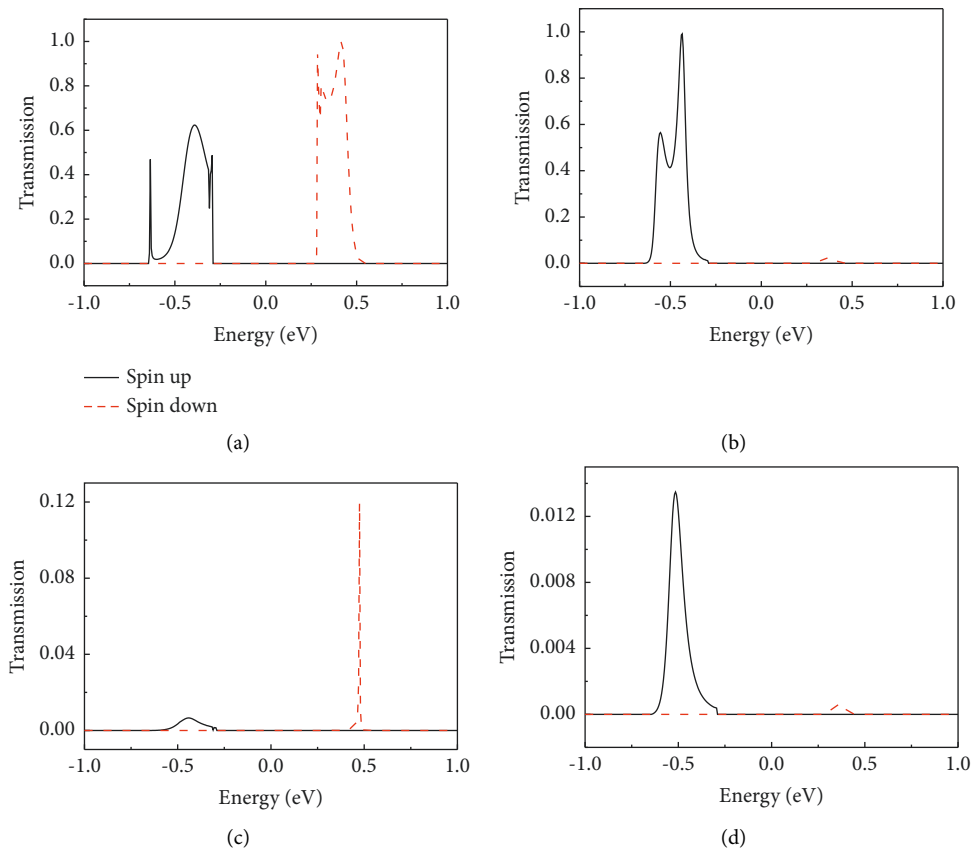

Figure 2: The spin-dependent TS of the thermal spin device, (a) R = CONH, closed state, (b) R = CONH, open state, (c) $R = CH_2$, closed state, and (d) $R = CH_2$, open state. The red and black lines indicate the SU and SD electrons, respectively.

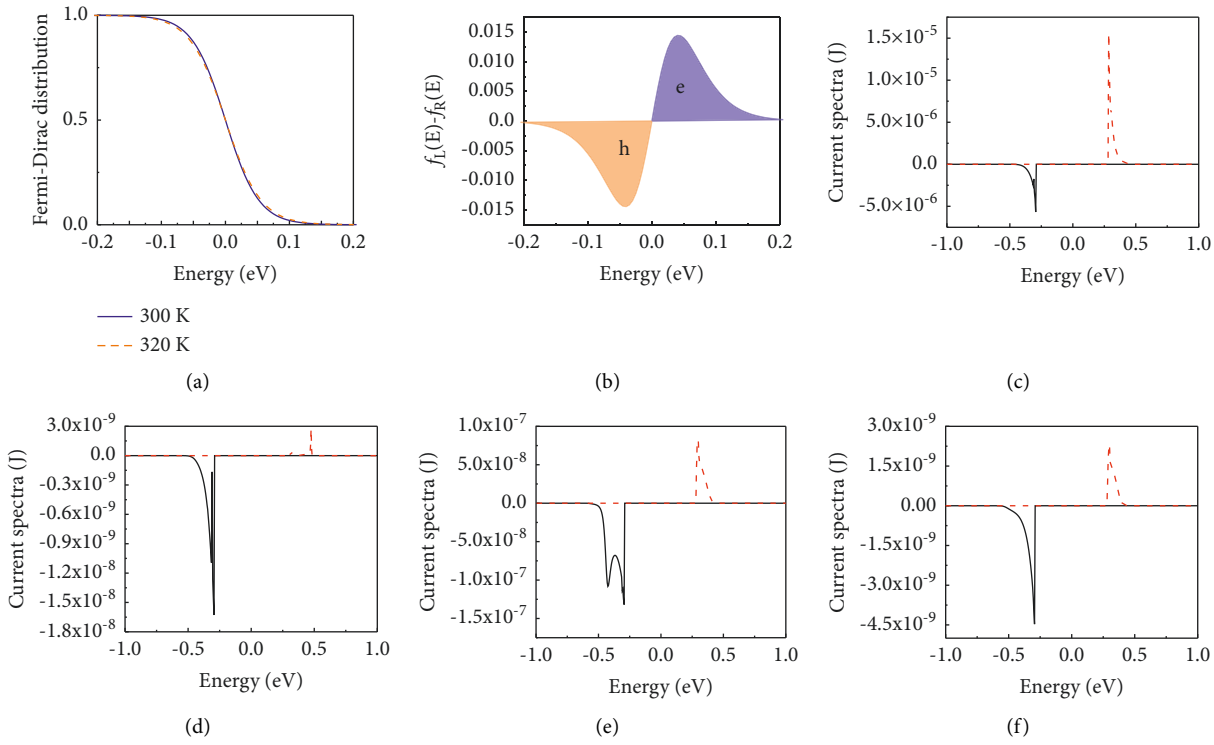

FIGURE 3: (a) The thermal spin device's Fermi distribution of the T_L and T_R. (b) The difference of Fermi functions ($T_L = 320$ K, TR = 300 K). The spin-related current spectra at $\Delta T = 20$ K and $T_L = 320$ K (c) $R = \mathrm{CONH}$, closed state, (d) $R = \mathrm{CONH}$, open state, (e) $R = \mathrm{CH_2}$, closed state, and (f) $R = \mathrm{CH_2}$, open state.

wider than that of open isomers. This heterogeneous distribution of TS leads to various transport capacities of the four forms.

In order to understand the primary structure of spin-related currents caused by the temperature difference, the current spectra $J(E)$ is first chosen as the multiplication of the TS and the Fermi functions difference $T^{\downarrow(\uparrow)}[f_L(E, T_L) - f_R(E, T_R)]$. Since the right and left electrodes have the same materials and state densities, the FDD $f_L(E, T_L) - f_R(E, T_R)$ indicates the carrier nature and concentration via the constructed device, relying on electron temperature at two leads, as presented in Figure 3(a).

The FDD function is described as $f_{L(R)}(E, T_{L(R)}) = \left\{1 + \exp[(E - \mu_{L(R)})/k_B T_{L(R)}]\right\}^{-1}$, where μ describes the chemical potential, taken as zero in our computation. As presented in Figure 3(b) (describing the FDD), the number of electrons on the right, including the energy higher than the FL, is more significant than on the left. Thus, the electrons move from the right to the left. Besides, the number of holes in the right, including the energy lower than the FL, is greater than in the left, while holes also move from the right to the left. The current spectra $J(E)$ of four devices are shown in Figure 3, where $\Delta T = 20$ K and $T_L = 320$ K, (c) R1, closed state, (d) R1, open state, (e) R2, closed state, and (f) R2, open state. The SD and SU current spectra $J(E)$ appear in a range of energies higher and lower than the FL, respectively. The current spectra $J(E)$ of closed isomers are tens of hundreds of times greater than those of open ones.

The obtained spin-related currents of R1 devices with respect to the left temperature (T_L) and temperature bias (ΔT) are presented in Figure 4. The obtained results in figures 4(a), 4(b), 4(d), and 4(e) belong to the closed and open isomers-based devices, respectively. As presented in Figures 4(a) and 4(d), the values of I_{up} and I_{dn} are negative and positive, respectively. It is evident that I_{up} and I_{dn} can be produced using ΔT without external voltage, caused by the holes and spin-splitting electrons moving from the right to the left. Significantly, the I_{up} and I_{dn} amplitudes are approximately similar in the total temperature area for closed isomers, meaning an SSE. The spin-dependent current characteristic of the open isomer (as shown in Figures 4(b) and 4(e)) is similar to the closed one, except for a coarse SSE.

Next, we verify the devices' optical thermal magnetoresistance varying from the closed state to the open one, derived from the relationship.

$$\mathrm{MR}^{\uparrow,\downarrow}(\%) = \frac{\left(I^{\uparrow,\downarrow}c - I^{\uparrow,\downarrow}o\right)}{I^{\uparrow,\downarrow}} \times 100, \tag{4}$$

where $I^{\uparrow,\downarrow}c$ and $I^{\uparrow,\downarrow}o$ stand for the SU/SD currents in the closed and open states, respectively. The MR of the R1 devices is shown in Figures 4(c) and 3(f). As we can see, $\mathrm{MR}^{\uparrow}$ varies from around 1.8×10^4 to 2.7×10^4, while $\mathrm{MR}^{\downarrow}$ varies from around 9.0×10^5 to 3.0×10^6 in the applied temperature range versus the left temperature (T_L). The $\mathrm{MR}^{\downarrow}$ varies from around 2.0×10^4 to 3.0×10^4, while $\mathrm{MR}^{\downarrow}$ varies from around

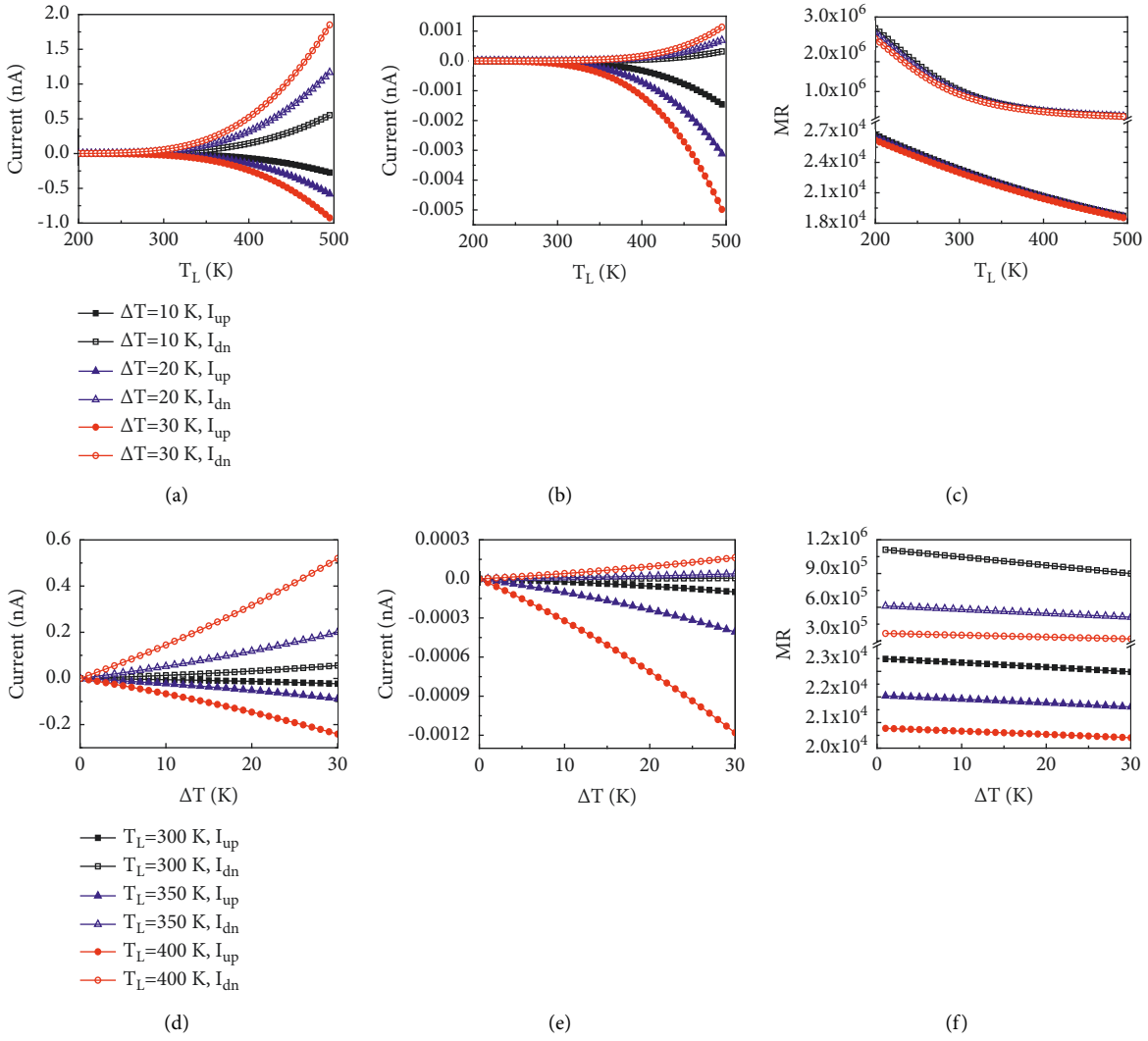

FIGURE 4: The thermally driven spin-related currents I_{up} and I_{dn} in the thermal spin devices (R = CONH) with respect to T_L and ΔT, (a) and (d) closed state; (b) and (e) open state. (c) and (f) the thermal spin devices' switching ratio versus T_L and ΔT, respectively.

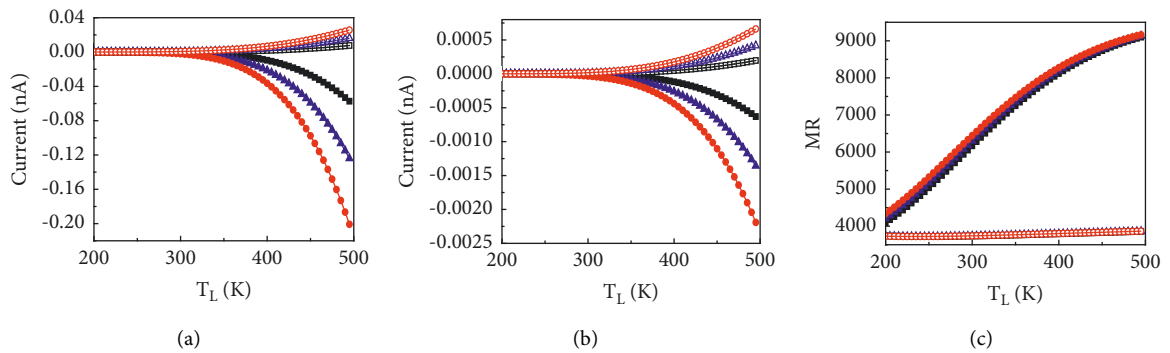

FIGURE 5: Continued.

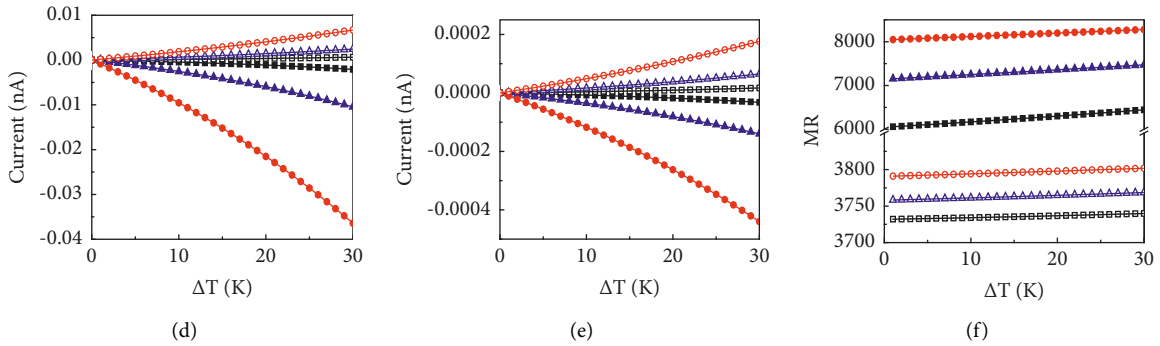

FIGURE 5: The thermally driven spin-related currents I_{up} and I_{dn} in the thermal spin devices ($R = CH_2$) versus T_L and ΔT, (a) and (d) closed state; (b) and (e) open state. (c) and (f) the corresponding switching ratio of the thermal spin devices versus T_L and ΔT, respectively.

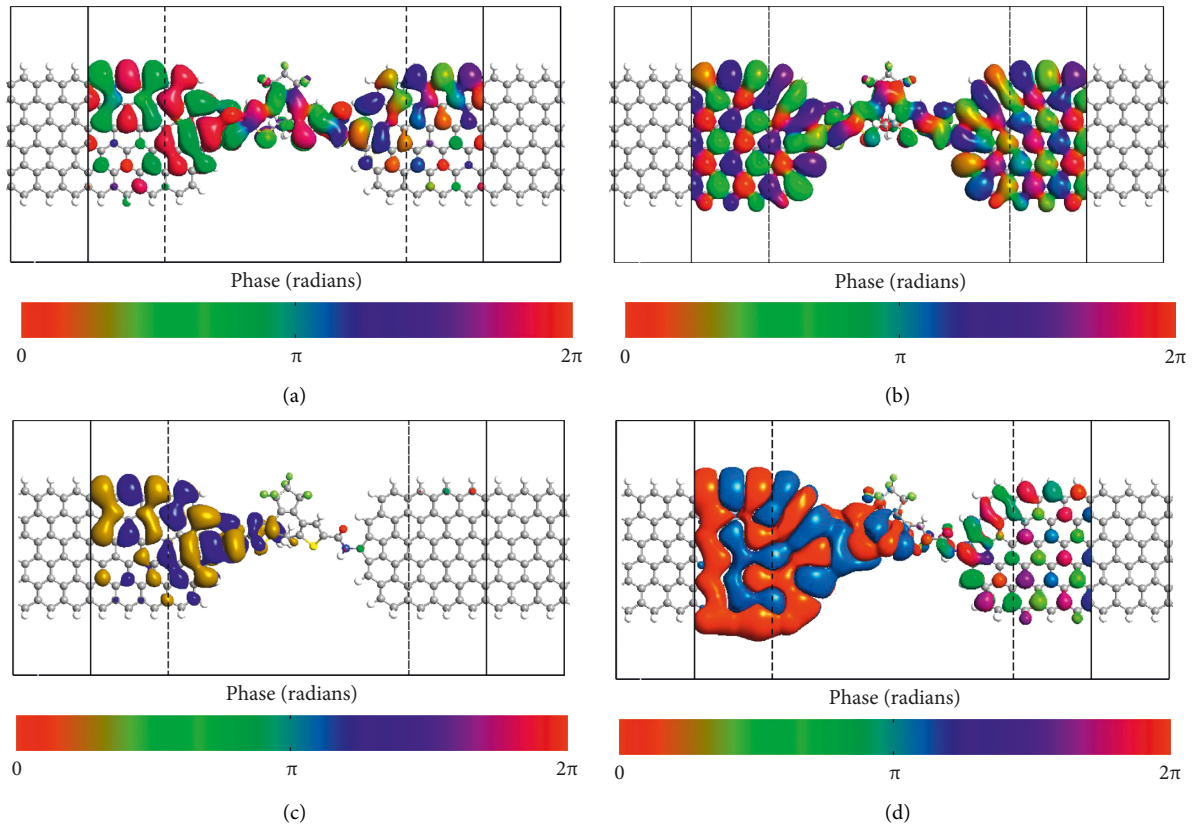

FIGURE 6: Spin-resolved transmission eigenstates of the thermal spin devices ($R = CONH$) under zero bias, (a) closed state, eV, (b) closed state, eV, (c) open state, eV, and (d) open state, eV. The isovalues are 0.1 $Å^{-3/2}$.

3×10^5 to 1.2×10^6 in the applied temperature range versus the temperature bias (ΔT).

Figure 5 describes the computed spin-related currents of the R2 device with respect to the source temperature (T_L) and temperature bias (ΔT). Results in Figures 5(a), 5(b) and 4(d), 4(e) belong to the closed and open isomers-based devices, respectively. R2 devices have similar laws to those of R1 devices but have smaller currents and on-off ratios.

In order to better describe the current magnitude, the transmission eigenstates should also be utilized. The transmission eigenstates for the R1 and R2 devices are presented in Figures 6 and 7 (the energies are marked with "$*$" in Figure 2), respectively. As described in Figures 6 and 7, the eigenstates are distributed more unlocally for $I^{\uparrow}$, $I^{\downarrow}$ of the R1 closed state, and $I^{\downarrow}$ of the R2 closed state. Meanwhile, the transmission eigenstates of the rest currents have a significant amplitude around the left electrode, which will decay from the left electrode to the right electrode. Notably, it disappears near the right electrode. Accordingly, the closed state currents are more significant than open states.

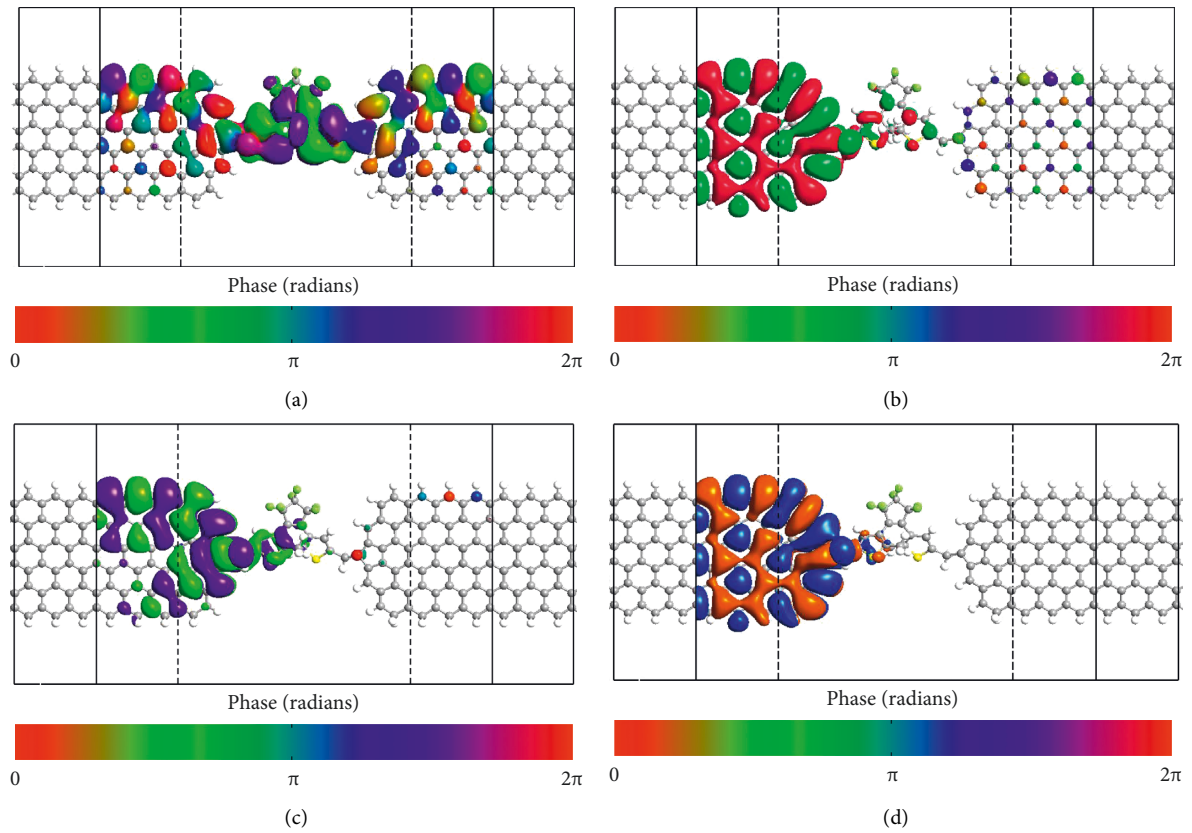

FIGURE 7: Spin-resolved transmission eigenstates of the thermal spin devices ($R = CH_2$) under zero bias, (a) closed state, eV, (b) closed state, eV, (c) open state, eV, and (d) open state, eV. The isovalues are 0.1 $Å^{-3/2}$.

4. Conclusions

An advanced spin caloritronic device is constructed using a diarylethene switch sandwiched between two semi-infinite zigzag graphene nanoribbons containing asymmetrical edge hydrogenation electrodes. By applying a temperature gradient to violate the electron-hole symmetry in the ZGNRs, SU and SD currents were produced with reverse transport orientations and the same order of magnitudes, indicating the appearance of the SSE. Moreover, the SU and SD currents are considerably dissimilar for two photochromic isomers at different temperature gradients, demonstrating the excellent system's switching action. The obtained outcomes disclose that light can control the thermal spin transport properties.

Data Availability

The data used to support the findings of this study are available on request from the authors.

Conflicts of Interest

The authors declare that they have are no conflicts of interest.

Acknowledgments

This work was supported by the National Natural Science Foundation of China with grant no. 11864011, in part by the Science and Technology Research Program of Chongqing Municipal Education Commission (KJQN202101204).

Supplementary Materials

Supporting Information is available from the Hindawi Online Library or from the author. Figure S1: The band structures of 6-ZGNRs. The red and black lines indicate the spin-down and spin-up electrons, respectively. (*Supplementary Materials*)

References

[1] M. Zeng, Y. Feng, and G. Liang, "Graphene-based spin caloritronics," *Nano Letters*, vol. 11, no. 3, pp. 1369–1373, 2011.

[2] D.-D. Wu, H.-H. Fu, Q.-B. Liu, and R. Wu, "How to realize the Spin-seebeck effect with a high spin figure of merit in magnetic boron-nitrogen nanoribbon and nanotube structures?" *Journal of Materials Chemistry C*, vol. 6, no. 39, pp. 10603–10610, 2018.

[3] K. Uchida, J. Xiao, H. Adachi et al., "Spin seebeck insulator," *Nature Materials*, vol. 9, no. 11, pp. 894–897, 2010.

[4] K. Uchida, S. Takahashi, K. Harii et al., "Observation of the Spin seebeck effect," *Nature*, vol. 455, no. 7214, pp. 778–781, 2008.

[5] X. Tan, L. Ding, G.-F. Du, and H.-H. Fu, "Spin caloritronics in two-dimensional $CrI_3/NiCl_2$ van der Waals heterostructures," *Physical Review B*, vol. 103, no. 11, Article ID 115415, 2021.

[6] H.-H. Fu, D.-D. Wu, L. Gu, M. Wu, and R. Wu, "Design for a Spin-seebeck diode based on two-dimensional materials," *Physical Review B*, vol. 92, no. 4, Article ID 045418, 2015.

[7] S. R. Boona, R. C. Myers, and J. P. Heremans, "Spin caloritronics," *Energy & Environmental Science*, vol. 7, no. 3, pp. 885–910, 2014.

[8] G. E. W. Bauer, E. Saitoh, and B. J. van Wees, "Spin caloritronics," *Nature Materials*, vol. 11, no. 5, pp. 391–399, 2012.

[9] Y. Ni, K. Yao, H. Fu, G. Gao, S. Zhu, and S. Wang, "Spin seebeck effect and thermal colossal magnetoresistance in graphene nanoribbon heterojunction," *Scientific Reports*, vol. 3, no. 1, p. 1380, 2013.

[10] H.-H. Fu, D.-D. Wu, G.-F. Du, Q.-B. Liu, and M. Wu, "Low energy dissipation readout of single-molecule ferroelectronic states by a Spin-seebeck signal," *Physical Review Research*, vol. 2, no. 4, Article ID 043406, 2020.

[11] M. Irie, T. Fukaminato, T. Sasaki, N. Tamai, and T. Kawai, "A digital fluorescent molecular photoswitch," *Nature*, vol. 420, no. 6917, pp. 759-760, 2002.

[12] S. Nakamura, S. Yokojima, K. Uchida, and T. Tsujioka, "Photochromism of diarylethene: effect of polymer environment and effects on surfaces," *Journal of Photochemistry and Photobiology C: Photochemistry Reviews*, vol. 12, no. 2, pp. 138–150, 2011.

[13] M. Irie, S. Kobatake, and M. Horichi, "Reversible surface morphology changes of a photochromic diarylethene single crystal by photoirradiation," *Science*, vol. 291, no. 5509, pp. 1769–1772, 2001.

[14] S. Kobatake, S. Takami, H. Muto, T. Ishikawa, and M. Irie, "Rapid and reversible shape changes of molecular crystals on photoirradiation," *Nature*, vol. 446, no. 7137, pp. 778–781, 2007.

[15] N. Katsonis, M. Lubomska, M. M. Pollard, B. L. Feringa, and P. Rudolf, "Synthetic light-activated molecular switches and motors on surfaces," *Progress in Surface Science*, vol. 82, no. 7-8, pp. 407–434, 2007.

[16] S. Jan van der Molen and P. Liljeroth, "Charge transport through molecular switches," *Journal of Physics: Condensed Matter*, vol. 22, no. 13, Article ID 133001, 2010.

[17] C. Motta, M. I. Trioni, G. P. Brivio, and K. L. Sebastian, "Conductance of a photochromic molecular switch with graphene leads," *Physical Review B*, vol. 84, no. 11, Article ID 113408, 2011.

[18] C. Jia, A. Migliore, N. Xin et al., "Covalently bonded single-molecule junctions with stable and reversible photoswitched conductivity," *Science*, vol. 352, no. 6292, pp. 1443–1445, 2016.

[19] M. Brandbyge, J.-L. Mozos, P. Ordejón, J. Taylor, and K. Stokbro, "Density-functional method for nonequilibrium electron transport," *Physical Review B*, vol. 65, no. 16, Article ID 165401, 2002.

[20] A. ToolKit, "QuantumWise A/S," 2014, https://www.quantumwise.com.

[21] J. P. Perdew and Y. Wang, "Accurate and simple analytic representation of the electron-gas correlation energy," *Physical Review B*, vol. 45, no. 23, pp. 13244–13249, 1992.

[22] J. P. Perdew, K. Burke, and M. Ernzerhof, "Generalized gradient approximation made simple," *Physical Review Letters*, vol. 77, no. 18, pp. 3865–3868, 1996.

[23] Y. Imry and R. Landauer, "Conductance viewed as transmission," *Reviews of Modern Physics*, vol. 71, no. 2, pp. S306–S312, 1999.

[24] L. M. Sandonas, H. Sevinçli, R. Gutierrez, and G. Cuniberti, "First-principle-based phonon transport properties of nanoscale graphene grain boundaries," *Advancement of Science*, vol. 5, no. 2, Article ID 1700365, 2018.

[25] M. Saiz-Bretín, L. Medrano Sandonas, R. Gutierrez, G. Cuniberti, and F. Domínguez-Adame, "Impact of device geometry on electron and phonon transport in graphene nanorings," *Physical Review B: Condensed Matter*, vol. 99, no. 16, Article ID 165428, 2019.

[26] J. C. W. Song, M. Y. Reizer, and L. S. Levitov, "Disorder-assisted electron-phonon scattering and cooling pathways in graphene," *Physical Review Letters*, vol. 109, no. 10, Article ID 106602, 2012.

[27] D. Gunlycke, H. M. Lawler, and C. T. White, "Room-temperature ballistic transport in narrow graphene strips," *Physical Review B: Condensed Matter*, vol. 75, no. 8, Article ID 085418, 2007.